Journal of Materials Chemistry C

Accepted Manuscript

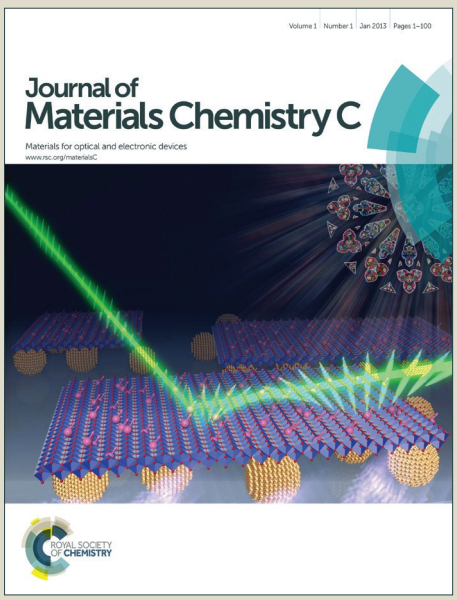

ROYAL SOCIETY OF CHEMISTRY

www.rsc.org/materialsC

Facile Preparation of Graphite Particles Fully Coated with Thin Ag Shell Layers for High Performance Conducting and Electromagnetic Shielding Composite Materials

Yilong Wang,†[ab] Shigang Luo,†[a] Ke Ren,†[a] Suling Zhao,*[c] Zhihong Chen,[d] Wei Li[a] and Jianguo Guan*[a]

[a] State Key Laboratory of Advanced Technology for Materials Synthesis and Processing, Wuhan University of Technology, Wuhan 430070, P. R. China. *E-mail: guanjg@whut.edu.cn

[b] School of Chemistry, Chemical Engineering and Life Science, Wuhan University of Technology, Wuhan 430070, P. R. China.

[c] Center for Material Research and Analysis, Wuhan University of Technology, Wuhan 430070, P. R. China. *E-mail: zhaosl@whut.edu.cn

[d] School of Science, Wuhan University of Technology, Wuhan 430070, P. R. China.

† These authors contribute equally to this paper.

Abstract: We have demonstrated a facile surface-functionalization method to achieve high density of thiol groups on natural graphite particles (NGPs), which fabricates compact silver shells of about 50 nm in thickness on the surface of NGPs by electroless silver plating. In our protocol, the addition of water and ammonia in the modification not only promotes the condensation of the free hydrolyzed 3-mercaptopropyltrimethoxysilane (MPTMS) molecules with the hydroxyl groups on NGPs, but also enhances the self-polymerization of them with MPTMS grafted on NGPs. In this way, simply optimizing the volume ratio of H_2O to MPTMS ($V_{H_2O}:V_{MPTMS}$) in the modification can make density of thiol groups (N_{SH}) on the surface of NGPs be as high as ~ 52 -SH groups per nm^2, which subsequently produces thin and compact silver shells on NGPs by creating dense Ag nuclei. Compared with the previously reported silver-coated non-metallic core-shell composite particles, the as-synthesized NG@Ag core-shell composite particles (NG@Ag CSCPs) show a big conductivity of 1.71×10^6 S/m even when the Ag content is as low as 32 wt.%, implying the advantages of low density, high thermal stability and low cost. The polymer-based composite materials based on them exhibit excellent conductivity, strong shielding effectiveness and good anti-sedimentation, as well as the good mechanical properties, conducting stability and small filling volume percentage, suggesting that the as-synthesized NG@Ag CSCPs are promising for the application in the conductive and electromagnetic shielding composite materials fields.

Introduction

Core-shell composite particles consisting of non-metallic cores covered with compact silver shells have recently attracted much attention in many fields including conductive composite material,[1, 2] electromagnetic interference (EMI),[3] photocatalysis,[4] catalysis[5] and surface-enhanced Raman scattering (SERS) .[6, 7] This is because the silver shell shows big conductivity (i.e. 6.3×10^7 S/m), unique optical properties and surface plasmon resonance, while the non-metallic cores, such as glass microspheres,[8] carbon[9] and polystyrene (PS),[10, 11] have low density, good chemical stability, cheap cost and easy availability. Besides the combination of these advantages stemming from their single-component counterparts, the core-shell composite particles may further exhibit some modified and improved properties depending on the core-to-shell ratio.[12] Up to now, there are numerous methods to be developed to fabricate such well-defined silver-coated non-metal core-shell composite particles, including electrodeposition,[13] ultrasound irradiation[14] and hydrothermal method.[15] However, owing to the scarce active sites on the cores for heterogeneous nucleation of Ag atoms, these methods generally suffer from homogeneous nucleation of Ag,[16] leading to the formation of the separated Ag nanoparticles or incomplete shells coverage among the as-synthesized composite particles. These issues originate from the considerable surface free energy differences and the insufficient wetting between the non-metallic core and silver. More recently, the developed layer-by-layer (LBL) self-assembly,[17, 18] seed-mediated growth,[10, 19-21] polydopamine (PDA) modification[22, 23] or thiol-functionalization coupled with electroless silver plating[7, 11]

have focused on improving the interface affinity between cores and silver shells in order to obtain the continuous and compact shells on cores. Nevertheless, the currently reported core-shell composite particles have thick shells[10, 22] (*e.g.* >100 nm in thickness), high silver content (≥55.03 wt%) and high density, resulting in their sedimentation or underdeveloped dispersity in polymer matrix.[20] These issues seriously impose restrictions on the application of these silver-coated core-shell composite particles in conductive or EMI polymer-based composite materials. Consequently, it is necessary to design and fabricate silver-coated non-metal core-shell composite particles with thin and compact silver shells.

To address these obstacles, some materials with abundant active functional groups (i.e. hydroxyl group), such as SiO_2[7] and TiO_2,[24] were performed as cores to fabricate the resulting composite particles. For the preparation principle of these methods, it can be explained by the fact that these materials could either directly absorb vast positively-charged silver precursor[7] or provide a great number of hydroxyl groups to produce active sites where chemically attach Ag^+ ions. Subsequently, the Ag-containing compound may be *in situ* reduced to Ag^0 by reducing reagents. Then, the reduced silver atoms isotropically grow into Ag nuclei which induce more silver atoms to deposit on the surface of cores in the following process. Finally, the compact shells without any naked core form after the full growth of silver grains. Although these composite particles with the integrated Ag shells of about 50 nm in thickness were successfully synthesized by using surface-functionalization or electrostatic attraction coupled with electroless deposition technique, the as-synthesized composite

particles tend to exhibit excellent performances in the fields of SERS for label-free detection of the pesticides in the fruit samples or solar power.[7, 24] Additionally, the inner-cores of these composite particles are neither conductive fillers nor anisotropic ones, resulting in the relatively small conductivity and high filling volume percentage of their composite materials. The last but not the least, the diameters of the literature-reported silver-coated composite particles[7, 24] are too small to be suitable for the application of the conductive or EMI composite materials owing to their aggregation or difficulty of dispersity in the polymer matrix.

The graphite crystal lattice consists of graphene layers formed by sp^2 hybridized carbon atoms tightly bonded in six-member rings, while carbon sheets are bounded by weak van der Waals forces with each other.[25] Such a unique structure makes graphite show favorable electronic mobility in the graphene layer. In combination of a certain conductivity (~10^4 S/m), low percolation threshold in the polymer matrix because of its shape anisotropy,[26-28] light-weight, easy availability, large abundance and low cost,[29] NGPs have been widely used as a good candidate in fabricating polymer conducting composites or the negative electrode materials for lithium ion batteries. But the incomplete graphitization during the natural formation process often brings about some unnecessary structural defects such as sp^3-hybridized carbon atoms, edge atoms, carbon chains and oxygen functional groups,[30] resulting in the depression of their conductivity. In addition, NGPs can not be used as high performance conductive fillers, owing to large contact resistance (~ 10^3 $\Omega \cdot cm^2$) in the polymer matrix[31] and unsatisfactory conductivity in comparison with silver fillers. NG@Ag CSCPs with

intact silver shells may address the above mentioned problems since they not only inherit the sheet structure and characteristics of NGPs, but also retain high conductivity and low contact resistance (68 $\Omega \cdot cm^2$) of silver fillers.[26, 32] As is well known, owing to insufficient active functional groups or inert surface of NGPs, the way of strong acid oxidation has been widely explored to produce a great many of oxygen-containing groups (for example, hydroxyl, carbonyl and carboxyl group) on NGPs, prior to achieving variously functionalized modifications on them. However, NGPs tends to be exfoliated by this acid/oxidation method, just like graphene layers were deposited by mechanical, physical or ultrasonic exfoliation from graphite. In this manner, it leads to the sharp increasing of specific surface area of graphite sheets, which has to consume a large amount of silver precursors to form complete shells on them in the following electroless plating and results in high silver content or high density of the resultant composite particles as well. As a result, graphene, graphene oxide or the reduced graphene oxide, high specific surface area inner-core particles, are not appropriate for using as cores to synthesize such the composite particles with compact silver shells. Given the above, the so far synthesized NG@Ag CSCPs generally either have an incomplete coverage and separated silver nanoparticles due to the insufficient active functional groups on inert surface of NGPs,[19] or the relatively high Ag content and large density of the final composite particles.[33, 34] Therefore, it is urgent to develop an effective, simple and versatile method for the deposition of thin and compact Ag shells on NGPs.

Herein, we have for the first time developed a facile surface-functionalization

strategy for grafting dense thiol groups on the surface of NGPs by simply tuning $V_{H_2O}:V_{MPTMS}$ with ammonia as catalyst in the modification, which can serve as the intermediate medium to deposit thin and compact Ag shells on NGPs. The increase in N_{SH} substantially enhances the density of silver nuclei (N_{Ag}), resulting in compact shells with the relatively thin thickness on NGPs. The as-synthesized NG@Ag CSCPs, with silver content of 32 wt.% and density of 3.06 g/cm^3, have the compact shells of about 50 nm in thickness. Furthermore, we proposed a rationally stepwise formation mechanism to explain the sensitivity of the shell thickness or morphology of NG@Ag CSCPs to $V_{H_2O}:V_{MPTMS}$ in the modification. Compared with other prepared nonmetal@Ag core-shell composite particles, the resultant composite particles have big conductivity, low Ag content, low density and high thermal stability, besides strong shielding effectiveness, good anti-sedimentation, excellent mechanical properties, stability of conductivity and low filling volume percentage of their composite materials, suggesting that the as-synthesized NG@Ag CSCPs and their composite materials can be widely used in the fields of conductive and electromagnetic shielding.

Experimental section

Materials

Natural graphite particles (NGPs, 99% purity) were purchased from Qingdao Jin Rilai Graphite Co., Ltd., Shandong province, China. 3-mercaptopropyltrimethoxysilane (MPTMS) was purchased from Wuhan University

Silicone New Material Co., Ltd., Hubei province, China. Flaky silver powders (PA-1) with the average diameter of 6 μm were purchased from Kunming Hendera Science and Technology Co., LTD., Yunnan province, China. The commercial glass microspheres@Ag core-shell composite particles with an average diameter of 45 μm were purchased from Potters Industries Inc, USA. Other chemicals including silver nitrate, polyvinylpyrrolidone (PVP, K30), ethanol, ammonia, sodium hydroxide, glucose and potassium sodium tartrate were all purchased from Sinopharm Chemical Reagent Co., Ltd., Shanghai, China. These chemicals were of analytical reagent grade and used without further purification. Deionized water with a resistivity of 18 MΩ·cm was used in the described reactions. Prior to using NGPs, they should be rinsed by soxhlet extraction to remove some impurities such as kerosene and vegetable oil. The rinse of NGPs consists of two steps: (i) 30.0 g NGPs were extracted with 200.0 mL of ethanol-water mixture (volume ratio of 1:1) for 6 h in a 500 mL soxhlet apparatus; (ii) NGPs were further washed with ethanol for three times, followed by filtration and drying at 60 ^{o}C for 2 h.

Functionalization of NGPs by silane coupling agent

In the typical experiment, 2.50 g NGPs were dispersed into the mixture solvent containing of 82.0 mL ethanol and 18.0 mL water with vigorous magnetic stirring, followed by adding 0.50 mL MPTMS and 2.00 mL $NH_3 \cdot H_2O$. The reaction mixture was maintained at 60 ^{o}C for 6 h. The concentrations of MPTMS, ammonia and H_2O were 0.026, 0.14 and 10.54 mol/L in the mixed solution, respectively. The reactant was filtrated, washed with ethanol for three times, and finally dried at 60 ^{o}C for 2 h to

obtain MPTMS-functioned natural graphite particles (MNGPs).

Preparation of NG@Ag CSCPs

The silver precursor aqueous solution (denoted as solution A) consists of 3.40 wt.% $AgNO_3$, 4.48 wt.% $NH_3 \cdot H_2O$ and 2.00 wt.% NaOH. The volume of solution A is abbreviated to V_A. Another aqueous solution containing 4.00 wt.% glucose and 0.35 wt.% potassium sodium tartrate was heated to the boiling point for 5 min and then cooled down to room temperature to obtain the reducing aqueous solution, which is denoted as solution B. In the typical experiment, 0.20 g PVP and 1.00 g MNGPs were successively added into a 100-mL plastic beaker containing 40.0 mL of solution B with vigorous magnetic stirring. Then, 25.0 mL of solution A were dropped into the above reaction mixture with the dropping rate of 1.50 mL/min at room temperature. After finishing dropping, the reaction was allowed to last for *ca.* 30 min. Finally, the solid products were filtrated, washed with deionized water and ethanol respectively for three times, and dried at 60 ^oC for 2 h to obtain NG@Ag CSCPs.

Preparation of electrically conductive adhesives (ECAs)

The epoxy resin adhesives were prepared according to our previous work.[35] The details about ECAs are described as follows: 5.00 g epoxy resin and 3.50 g amino-terminated polyether crosslinking agent and NG@Ag CSCPs were fully dispersed by stirring, and then were coated uniformly on the mylar substrate by a coating knife and finally solidified in an oven at 100 ^oC for 10 h. The volume fraction of NG@Ag CSCPs or silver powders in all ECAs was 25 vol.%. In comparison, ECAs containing 50 vol.% of commercial glass microspheres@Ag core-shell

composite particles were also prepared by same way.

Preparation of electromagnetic shielding coating materials (ESCMs)

15.00 g epoxy resin and 10.50 g amino-terminated polyether crosslinking agent, NG@Ag CSCPs and 20.00 g dimethylbenzene were fully dispersed by stirring, which was then sprayed on FR-4 panel and finally solidified in an oven at 100 ^{o}C for 10 h. The volume fraction of NG@Ag CSCPs in coating materials was still 25 vol.%. Another ESCMs containing same volume fraction of flaky silver powders was also prepared in this way. Both the thickness of ESCMs were tuned to about 150 μm by controlling the spray times. An engraving machine (Creation Tech. H.K., KX4060) with a highest resolution of 3.125 μm was used to pattern the as-obtained coating materials containing NG@Ag CSCPs or flaky silver powders into the annular wafers which have outer radius of 55.00 mm and inner radius of 6.25 mm.

Characterizations

The density of hydroxyl groups on the surface of NGPs was determined by direct acid-based titrations.[36, 37] Before titration, the electrode of the PHS-2F meter was calibrated by buffer solutions with pH = 6.86 and 4.00, respectively. The pH value of the titration system was monitored by this PHS-2F meter. All titrations were carried out at room temperature using 1.00 g cleaned NG and 70.0 mL deionized water. During the titration, Ar gas was flushed through the liquid to avoid dissolving of CO_2 into the solution. Titrations of NGPs started after the addition of 5.00 mL oxalic acid (1.00 mmol/L) to the titration system. When the pH value of the titration system reached up to a constant value, 10.00 mmol/L NaOH solution with a constant velocity

of 0.25 mL min^{-1} was added dropwise into the above mixture. At the endpoint of the titration, the pH value increased to 10.20. Also a blank experiment consisting of 70.0 mL deionized water and 5.00 mL oxalic acid was titrated in the same way. The above two experiments were repeated for three times. Then，titration curve about pH versus V_{NaOH} was obtained.

The morphologies of the pristine NGPs and NG@Ag CSCPs were studied by a field emission scanning electron microscope (FESEM, Hitachi S-4800) operating at an accelerating voltage of 10.0 kV. The shell thickness of NG@Ag CSCPs was measured for 10 times to calculate its average value. The element composition of NG@Ag CSCPs was characterized by a Horiba EX-250 X-ray energy-dispersive spectrometer (EDX) associated with FESEM. The phase purity of the products was examined by X-ray diffraction (XRD) pattern obtained via Rigaku D/max-III A diffractometer with Cu Kα radiation (λ = 0.15418 nm) in the 2θ range from 10 ° to 80 ° at a scanning step of 0.02 °. Thermal analysis was conducted on a NETZSCH STA 449 C instrument under N_2 at a heating rate of 10 ℃ min^{-1}. X-ray photoelectron spectroscopy (XPS) measurements were performed on a VG Multilab 2000 X XPS system with Al Kα source. All the binding energies were referenced to the C1s peak at 284.8 eV of the surface adventitious carbon.

Brunauer-Emmett-Teller (BET) specific surface area was measured by an ASAP 2020 Micromeritics analyzer. All the as-prepared samples were degassed at 180 ℃ prior to nitrogen adsorption measurements. The BET specific surface area was determined by a multipoint BET method using the adsorption data in the relative

pressure (p/p_0) ranging from 0.05 to 0.3. Elemental analysis was performed by combustion and gas chromatographic analysis with a Vario EL cube CHNSO analyzer from Elementar. Each sample was measured for three times to calculate its average value. The density of NG@Ag CSCPs was determined by using a pycnometer with 10.00 mL in volume.

Measurements of electrical conductivity

The electrical conductivities of the products (including NG@Ag CSCPs, their ECAs and ESCMs) were measured by the Four-Point-Probe system (5601-Y source measure unit, Qitai Corp., Taiwan) for 5 times to calculate the average value. The spacing between the tips was 1.00 mm. Before the measurement of NG@Ag CSCPs, they were pressed into a tablet with about 1.0 mm in thickness with a pressure of 10.0 MPa for 10 minutes.

Measurements of shielding effectiveness

According to SJ 20524-1995 (Measuring Methods for Shielding Effectiveness of Materials), the coaxial fixture (DN1015A, to be purchased from EMC LAB of Southeast University, Nanjing, Jiangsu province, China) was connected to an Agilent N5230A Vector Network Analyzer (VNA) to measure shielding effectiveness (*SE*) of these ESCMs.

RESUTS AND DISCUSSION

Figure 1 represents the morphology, phase analysis and composition information of NG@Ag CSCPs synthesized in the typical experiment and the morphology of NGPs.

It can be seen that NGPs are well dispersed and variable in size, as shown in Figure 1a. The average diameter of NGPs is *ca*. 42.8 μm in Figure S1 (ESI†). The inset of Figure 1a suggests that NGPs have the uneven surface with some tiny particles. Figure 1b indicates that there is no separated or agglomerated silver nanoparticle in the resultant composite particles, and the as-synthesized NG@Ag CSCPs do not show any considerable difference in the dispersity from NGPs. Furthermore, the as-synthesized composite particles almost have the same size as NGPs. The EDX analysis and XRD pattern confirm the composition and crystal structure of the composite particles. As is shown in Figure 1c, the composite particles are composed of C, O, Si, S and Ag elements. The Si and S elements should be from MPTMS molecules that were chemically bonded on the surface of NGPs after the modification. From the XRD pattern of the composite particles (Figure 1d), the diffraction peaks locating at 2θ = 26.4 ^{o} and 54.5 ^{o} correspond to planes (002) and (004) of NGPs, respectively, while other peaks at 2θ =38.1 ^{o}, 44.3 ^{o}, 64.5 ^{o} and 77.4 ^{o} are the diffraction from planes (111), (200), (220) and (311) of *fcc* structure of silver in turn (JCPDS Card No.4-783). No other crystalline impurity is detected, demonstrating the purity phase of silver formation on NGPs. The average grain size of silver crystallites in the final solid products is calculated to be about 21.0 nm according to Debye-Scherrer equation. Compared with the inset of Figure 1a, the compact silver shell of the composite particles is clearly observed in Figure 1e. It is worthy of notice that the as-synthesized Ag shells on NGPs in our protocol is more compact than that prepared with the seed-mediated growth method.[19, 33] From Figure 1f, the as-synthesized Ag shells on

NGPs are still compact even when the thickness is as thin as about 50 nm. We can reasonably speculate about the assumption that the Ag shells of NG@Ag CSCPs have the polycrystalline structure and are composed of two and a half layers of silver crystallites. The thickness of silver shells (d_{Ag}) on non-metallic cores with low reactivity using the so far reported synthesis approaches, is far thicker than that of the as-synthesized composite particles in typical experiment. Some quintessential examples should be cited that, the compact silver shells have been reported to be about 110 nm in thickness for PS@Ag composite particles,[10] and about 490 nm of shell thickness for PMIA@Ag composite fiber,[22] respectively. From the above results, NG@Ag CSCPs with thin and compact shells are successfully synthesized in this paper. Furthermore, the hydroxyl group density of NGPs is only about 0.94 nm^{-2} (Figure S2 and Table S1, ESI†), which is exactly much lower than those of TiO_2 (~ 10 nm^{-2})[38] SiO_2[39], ZrP[40], and so on (see Table S1, ESI†). As is mentioned above, it is generally very difficult to achieve thin and compact Ag shells on such substrate with inert surface using the currently reported methods owing to the lack of sufficient active sites for tethering dense silver nuclei.

In this approach, it is crucial to graft dense thiol groups onto the surface of NGPs as the intermediate medium to fabricate NG@Ag CSCPs with uniform and compact shells. Figure 2 presents the XPS spectra of NGPs functionalized by MPTMS molecules in the typical experiment. It can be seen that four peaks at the binding energy of 533.0, 285.0, 164.0 and 103.0 eV in Figure 2a are indexed to be the characteristic peaks of O 1s, C 1s, S 2p and Si 2p, respectively. In Figure 2b, the peak

of S can be attributable to S $2p_{1/2}$ and S $2p_{3/2}$ with binding energy position of 165.4 and 164.2 eV, respectively. In accordance with the rules of quantum mechanics, the peak area ratio and the difference in binding energy of S $2p_{1/2}$ and S $2p_{3/2}$ peaks are 2:1 and 1.2 eV, respectively, indicating that thiol groups had been successfully grafted onto the surface of NGPs.[41] In Figure 2c, the peak of Si 2p consists of three components.[42] Among them, the peak at the binding energy of 103.5 eV is due to Si-O-Si bond which comes from the dehydration of hydrolyzed MPTMS molecules among each other on the surface of NGPs; the peak at 102.7 eV corresponds to the uncondensed Si-OH because of steric hindrance;[43] the last peak at 101.9 eV is assigned to be Si-O-C bond, suggesting that silanol groups directly condense with the hydroxyl groups on the surface of NGPs. Furthermore, Figure 2c also illustrates that the area in the peak of Si-O-Si or Si-OH bond is much larger than that of Si-O-C bond, implying that most MPTMS molecules chemically bonded onto the surface of NGPs undergo self-polymerization each other.

Figure 3 shows the thermogravimetric (TG) and differential thermogravimetry (DTG) plots of the pristine NGPs and MNGPs synthesized in the typical experiment. The weight of NGPs declines gradually from 100 to 1000 ^{o}C due to the thermal decomposition of the defects with various decomposition temperatures including sp^3-hybridized carbon atoms, edge atoms, carbon chains and oxygen functional groups.[30] As is shown in Figure 3, the weight loss of MNGPs can be divided into three steps. First, the mild weight loss ranging from 100 to 200 ^{o}C may be assigned to the labile oxygen functional groups,[44] while the two major weight losses of 200-400

and 400-700 °C correspond to the thermal decomposition of the thiol groups and the residual alkyl groups of MPTMS molecules, respectively.[40] After these weight losses, the grafted MPTMS molecules on NGPs would gradually decompose into the stable SiC_xO_y residue[45] and the weight loss does not contain the thermal dissociation of defects on NGPs. This can be explained by the protection of the grafted MPTMS molecules against the decomposition of defects on NGPs.[46] Once the temperature is over 700 °C, those stable residue on MNGPs will decompose gradually. The DTG curve of MNGPs from 200 to 700 °C has further been fitted with Gaussian function in Figure 3. In agreement with the previous reports[40], the first peak at 352.72 °C and the second at 492.15 °C are ascribed to thermal dissociation of thiol group and alkyl groups grafted on MNGPs, respectively. The related results of MNGPs fitted with Gaussian function from the its DTG curve are shown in Table 1. The peak area of the thiol groups (*Area* 1) is 21.41, while that of the residual alkyl groups (*Area* 2) is 27.40. As the total weight loss (ΔW_{total}) of MNGPs from 200 to 700 °C is 4.22 wt.%, the weight content of thiol groups (ΔW_{SH}) of MNGPs can be calculated to be 1.84 wt.% in term of equation (1) :

$$\Delta W_{SH} = \Delta W_{total} \times \frac{Area\,1}{Area\,1 + Area\,2} \qquad (1)$$

Table 1. The related results of MNGPs fitted with Gaussian function from the its DTG curve.

Funtional group	Decomposition temperature (°C)	Peak area	Weight content (wt.%)
-SH	352.72	21.41	1.84
$-(CH_2)_3-$	492.15	27.40	2.38

Combined with the BET specific surface area of NGPs (S_{BET}) in Figure S3 of 7.07 m^2/g, N_{SH} of MNGPs is calculated to be 48.61 nm^{-2} by equation (2) ,[47]

$$N_{SH} = N_A \times \frac{\Delta W_{SH}}{10^{18} \times S_{BET} \times M_{SH}} \qquad (2)$$

where N_A and M_{SH} are the Avogadro constant (6.02×10^{23} mol^{-1}) and the molar mass of thiol group (-SH, 33.07 g/mol), respectively. Compared with the values listed in Table S1, it suggests that the MNGPs synthesized in our protocol have much larger N_{SH} or silane density than other literature-reported trimethoxysilane-modified matrixes, whereas the pristine NGPs show the relatively insufficient active groups to matrixes.

To explain the originality of large N_{SH} of the as-synthesized MNGPs, we have proposed the possible grafting principle of thiol groups anchored on the surface of NGPs. A few of hydrolyzed MPTMS molecules are directly bonded on the substrate from Scheme 1, where only a single silicon hydroxyl group per silane molecule reacted with the hydroxyl group of the NGPs to form the covalent C-O-Si bonds *via* a

hydrolysis-condensation reaction. The other two silicon hydroxyl groups of MPTMS molecules bonded on the substrate also dehydrate with other free hydrolyzed MPTMS molecules, resulting in achieving large N_{SH} on the surface of NGPs. Among them, the distance between the neighboring hydroxyl groups on NGPs surface is about 10.31 Å apart, and is approximately twice larger than the bond length of Si-O (3.28 Å). In this case, one hydrolyzed MPTMS molecule can not simultaneously react with two or more hydroxyl groups on the surface of NGPs. Instead, the silane dendrimers anchored on the surface of NGPs could be generated by siloxane bonds (Si-O-Si). Consequently, the specific number of the grafted thiol groups on the surface of NGPs is much more than that of the hydroxyl groups on them. This assumption can be supported by the result of hydroxyl groups density on NGPs and XPS analysis of MNGPs mentioned above.

Table 2. Influences of various reaction parameters on the sulfur content (C_S) and N_{SH} of MNGPs.

Sample	MPTMS (mmol/L)	H_2O (mol/L)	Ammonia (mol/L)	$V_{H_2O}:V_{MPTMS}$	C_S (wt.%)	N_{SH} (nm^{-2})
MNGPs -1	5.0	10.54	0.14	748:1	0.38	10.11
MNGPs -2	13.0	10.54	0.14	196:1	1.08	28.74
MNGPs -3	26.0	10.54	0.14	39:1	1.94	51.62
MNGPs -4	26.0	0.00	0.14	0:1	0.03	0.80
MNGPs -5	26.0	0.78	0.14	3:1	0.66	17.56
MNGPs -6	26.0	37.09	0.14	138:1	2.13	56.67
MNGPs -7	26.0	10.54	0.00	39:1	0.04	1.06

To further verify the above proposed assumption that large N_{SH} of MNGP originates from the self-polymerization of the grafted MPTMS molecules on the surface of NGPs with the free hydrolyzed ones, we have systematically investigated influences of various reaction parameters (including concentrations of MPTMS, H_2O and ammonia) on C_S or N_{SH} of MNGPs. Table 2 indicates that, with the concentration of MPTMS (C_{MPTMS}) increasing from 5.0 to 26.0 mmol/L, C_S increases while S_{BET} decreases to 6.89 m^2 g^{-1} (denoted as MNG-3, Figure S3, ESI†). It suggests that the grafted MPTMS molecules fill some pinholes on NGPs, leading to decreasing S_{BET}

and nitrogen sorption capacity of MNGPs.[46] Further increasing C_{MPTMS} to 52.0 mmol/L results in the aggregation of MNGPs (Figure S4b, ESI†), and significant decreasing S_{BET} of MNG to 1.66 m^2 g^{-1} (denoted as MNG-8, Figure S3, ESI†). When the concentration of water (C_{H_2O}) increases from 0.78 to 10.54 mol/L, C_S increases from 0.66 to 1.94 wt.%. Therefore, increasing C_{H_2O} not only accelerates the hydrolysis of MPTMS molecules to cause them to be grafted on the substrate *via* the dehydration with the hydroxyl groups on the surface of NGPs, but also results in the self-polymerization to start between the other two silicon hydroxyl groups unreacted of these grafted MPTMS molecules on the surface of NGPs and silicon hydroxyl groups of the free hydrolyzed MPTMS molecules in the modification.[48] This result also confirms the possible grafting principle of thiol groups anchored on the surface of NGPs in our protocol, as is mentioned in Scheme 1. However, further increasing C_{H_2O} to 37.09 mol/L leads to the aggregation of the resultant samples, the formation of silica nanoparticles (Figure S5, ESI†) and decreasing their S_{BET} to only 1.64 $m^2 \cdot g^{-1}$ (denoted as MNG-6, Figure S3, ESI†). According to C_S, N_{SH} on MNGPs can be calculated by equation (3) ,[47]

$$N_{SH} = N_A \times \frac{C_S}{10^{18} \times S_{BET} \times M_S} \qquad (3)$$

where M_S represents the molar mass (32.07 g/mol) of the sulfur element. In Table 2, the typical as-synthesized MNGPs have N_{SH} of 51.62 nm^{-2}, which is almost consistent with the analyzed result of 48.61 nm^{-2} from TG-DTG. However, C_S of MNGPs synthesized at C_{H_2O} = 0.00 mol/L or absolute ethanol (MNG-4) is only 0.03 wt.%, which converts to N_{SH} = 0.80 nm^{-2}. This value is approximately equal to the density of

hydroxyl groups on NGPs, suggesting that only a single methoxy group per silane reacts with the hydroxyl groups of the substrate and the other two methoxy groups remain unreacted.[43] On the other hand, ammonia is a traditional basic catalyst for silane condensation, and decreases the activation energy (E_a) for the dehydration of MPTMS with hydroxyl groups of the substrates and the self-polymerization of MPTMS molecules.[43] It plays an important role in the grafting dense thiol groups on NGPs in this work. The MNGPs synthesized at without ammonia as catalyst (MNG-7) have N_{SH} of about 1.06 nm^{-2}, which is also same as the density of hydroxyl groups on NGPs. Therefore, this result clearly demonstrates that the addition of water and ammonia in the modification is crucial to graft the large N_{SH} anchored on the surface of NGPs.

N_{SH} on MNGPs has a dominated influence on d_{Ag} of as-synthesized core-shell composite particles. At N_{SH} = 0.80 or 1.06 nm^{-2}, besides separated silver nanoparticles among these composite particles, agglomerated Ag islands stack on the surface of NGPs, which is obviously observed from Figures S6a and b. Some naked surface on MNGPs is uncoated by silver shells as well. It implies the occurrence of the homogeneous nucleation and growth of Ag atoms due to the lack of active sites for heterogeneous ones on MNGPs in these conditions. When N_{SH} increases to 10.11 nm^{-2} or above, compact silver shells form on the surface of MNGPs (insets of Figure S6c-e, ESI† and Figure 1e). At the same time, all these composite particles do not contain separated silver nanoparticles. They have good dispersity and the similar sheet structure to the pristine NGPs (Figure S6c-e, ESI† and Figure 1b). The shells of the

as-synthesized NG@Ag CSCPs can be qualified by the cross-section SEM images (Figure 4a-c and Figure 1f). From Figure 4d, d_{Ag} becomes thinner with increasing N_{SH} of MNGPs. At N_{SH} = 51.62 nm^{-2}, d_{Ag} decreases to *ca.* 50 nm. It suggests that dense N_{SH} benefits the formation of thin and compact silver shells on MNGPs.

In order to decipher how N_{SH} affects d_{Ag} or morphology of NG@Ag CSCPs, we have investigated the heterogeneous nucleation and growth of Ag atoms on the surface of MNGPs by electroless silver plating. For this purpose, only 1.00 mL of V_A is used for the deposition of Ag species on 1.00 g MNGPs to explore the influence of N_{Ag} on the surface of MNGPs. Figure 5 reveals that increasing N_{SH} tends to large N_{Ag} and makes the size of the Ag nanoparticles anchored on the MNGPs become small. Because the thiol group has a strong binding affinity for Ag via a soft Lewis acid-base interaction,[49] the substantial enhancement of N_{Ag} is carried out with increasing N_{SH} (Figure S7, ESI†). At N_{SH} = 28.74 nm^{-2}, N_{Ag} reaches up to ~ 1106 μm^{-2}, 1 to 2 orders of magnitude bigger than that obtained at N_{SH} = 0.80 nm^{-2}. This confirms that the higher N_{SH} , the higher N_{Ag}.[50]

Based on the above results, a possible formation mechanism of NG@Ag CSCPs with thin and compact silver shells is schematically illustrated in Scheme 2. In the first step of our protocol, NGPs are functionalized with MPTMS to graft thiol groups with the density regulated by simply changing V_{H_2O}:V_{MPTMS}. When V_{H_2O}:V_{MPTMS} = 0:1 (Scheme 2a), MPTMS molecules without water forms the sparse monolayer on NGPs through equation (4),[43] where only a single methoxy group per silane reacted with the surface hydroxyl groups of the substrate and the other two methoxy groups

remained unreacted due to higher activation energy (E_a).[43, 50, 51]

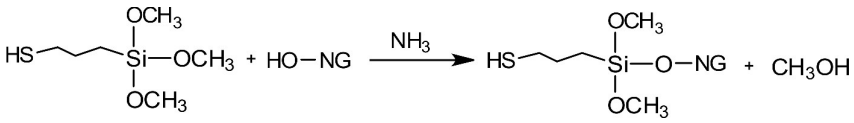

(4)

When $V_{H_2O}:V_{MPTMS}$ increases to 3:1, the hydrolysis of MPTMS molecules will occur. Then some of the hydrolyzed MPTMS molecules will dehydrate with hydroxyl groups on NGPs, and the others will undergo self-polymerization between each other to form some oligomers (Scheme 2b) according to equation (5)[52] and (6):[53]

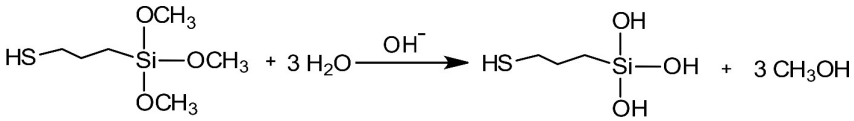

(5)

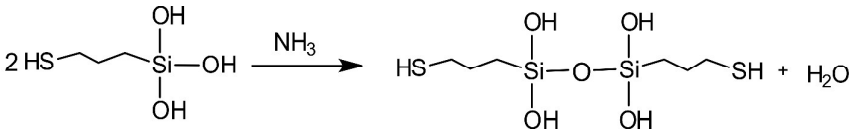

(6)

Further increasing $V_{H_2O}:V_{MPTMS}$ to 39:1 will accelerate the hydrolysis of MPTMS molecules and result in higher level of self-polymerization and larger N_{SH} on NGPs (Scheme 2c). In the subsequent electroless plating process, the heterogeneous nucleation and growth of Ag atoms is dependent upon N_{SH} of the surface of MNGPs. MNGPs with small N_{SH} (e.g. 0.80 nm^{-2}) tends to form the relatively small N_{Ag}, leading to uneven shells and separated silver nanoparticles. On the contrary, large N_{SH} (17.56 nm^{-2}) facilitates to form high N_{Ag} on MNGPs, and thus achieves the compact Ag shells. Larger N_{SH} (51.62 nm^{-2}) promotes denser N_{Ag}, resulting in the formation of thin and compact silver shells on MNGPs at last.

According to this formation mechanism, d_{Ag} is governed by N_{SH}, which can be simply regulated with changing $V_{H_2O}:V_{MPTMS}$ at ammonia as catalyst. Additionally, d_{Ag} can be also tailored by controlling V_A. For example, when V_A = 25.0 mL, the

as-synthesized NG@Ag CSCPs have the shells of about 50 nm in thickness, as shown in Figure 1f. If V_A increases from 34.0 to 64.0 mL, d_{Ag} increases from ~ 70 to ~120 nm, respectively (Figure S8, ESI†). The increase in d_{Ag} of NG@Ag CSCPs with increasing V_A is reasonably explained by the assumption that larger V_A can supply more Ag atoms for the growth of silver nuclei. In the following experiments, we would improve the electrical conductivity of ECAs containing NG@Ag CSCPs in this way.

Table 3. Comparison of silver content (C_{Ag}), density, shell morphology and electrical conductivity of NG@Ag CSCPs synthesized in the typical experiment and other silver-coated core-shell composite particles.

Core-shell composite particles	C_{Ag} (wt.%)	Density (g/cm^3)	Shell morphology	Electrical conductivity (S/m)	Ref.
PS@Ag-1	55.03	2.08[a]	uncompact	2.00×10^5	[10]
PS@Ag-2	77.10	3.43[a]	compact	1.77×10^6	[11]
PMIA@Ag	85.47	5.52[a]	uncompact	1.64×10^5	[22]
graphene@Ag	94.74	7.15[a]	uncompact	1.55×10^4	[54]
Graphite oxide@Ag	87.89	7.20[a]	uncompact	1.09×10^6	[33]
NG@Ag	32.00	3.06	compact	1.71×10^6	our work

[a] The density values were calculated by equation (7),

$$\rho_{\text{composite particles}} = \frac{1}{\frac{1-C_{Ag}}{\rho_{\text{core}}} + \frac{C_{Ag}}{\rho_{Ag}}} \quad (7)$$

where $\rho_{\text{composite particles}}$, ρ_{core} and ρ_{Ag} represent the density of composite particles, the inner-core particles and Ag, respectively (ρ_{core} = 1.05 g/cm^3 for PS[11], 1.46 g/cm^3 for

PMIA[55], 2.20 g/cm^3 for graphite oxide[56] and 1.06 g/cm^3 for graphene[57]; ρ_{Ag} = 10.49 g/cm^3 [11]).

Table 3 lists that the as-synthesized NG@Ag CSCPs with C_{Ag} of 32.00 wt.% have the electrical conductivity of 1.71×10^6 S/m. Its conductivity is much higher than that of the other silver-coated nonmetal core-shell composite particles,[10, 22, 33, 54] and is almost equivalent to that of the PS@Ag-2 core-shell composite particles whose C_{Ag} is as high as 77.10 wt.%. Moreover, the PS@Ag-2 core-shell composite particles have the relatively high density of 3.43 g/cm^3 [11] to NG@Ag CSCPs listed in Table 3. It is not difficult to understand that, according to equation (7), the thinner silver shells or less C_{Ag} form on NGPs, the smaller density of composite particles could be obtained. As is mentioned above, the high electrical conductivity of the as-synthesized NG@Ag CSCPs can be attributed to the compact silver shells on the surface of MNGPs from their SEM images. Table 3 further indicates that NG@Ag CSCPs have also the lower density (3.06 g/cm^3) than most of the core-shell composites particles, that is to say, conductive composite fillers. This is of significance for the fabrication of high performance conductive composite fillers with the small density differences between them and the polymer matrix (*ca.* 1.1-1.5 g/cm^3) may effectively prevent the sedimentation of the conductive composite fillers, which frequently occurs in the fabricating or processing of conductive and EMI polymer-based fillers-filled composite materials[20]. Figure 6 presents the XRD patterns of the as-synthesized NG@Ag CSCPs experiencing thermal treatment for 1 h at various temperature. No peak corresponds to silver oxides or other crystalline impurity, indicating that the composite particles inherit the excellent chemical stability of bulk Ag. In addition,

compared with one-dimensional silver nanostructures, such as silver nanowires,[58] NG@Ag CSCPs synthesized in our paper are easily obtained in a large-scale. Moreover, they may exhibit the conductivity comparable to that of the silver nanowires at low C_{Ag}, implying the advantages of low cost, as well as the small density and good dispersity in polymer matrix. These results suggest that the as-synthesized composite particles possess such advantages as big conductivity, high thermal stability and small density, all of which originate from the intrinsic characters of Ag, low C_{Ag}, the compact shells, as well as the anisotropic shape of NGPs.

As environmental awareness has increased, the commonly employed Sn/Pb solders have received negative attention due to their toxicity and overall adverse effect on our health. ECAs have been intensively researched as an alternative to solders in microelectronics.[26] The conductive fillers are one of important components in ECAs. To verify the performance of NG@Ag CSCPs, they are used as conductive fillers to prepare ECAs. Figure 7 shows the electrical conductivity of the ECAs containing 25.00 vol.% of NG@Ag CSCPs with various C_{Ag}. All the ECAs based on the as-synthesized composite particles show the conductivities higher than 1.5×10^4 S/m even when C_{Ag} of NG@Ag CSCPs is as low as 32.00 wt.%. The silver percent of ECAs consisting of NG@Ag CSCPs synthesized at C_{Ag} = 32.00 wt.% is only 14.50 wt.%. In contrast, those ECAs based on glass microsphere@Ag core-shell composite particles generally require a relatively high volume percentage (≥ 50.00 vol.%) when they have almost the same electrical conductivity as ECAs of the as-synthesized composite particles at C_{Ag} = 32.00 wt.% in our work. Out of expectation, increasing

C_{Ag} of the as-synthesized composite particles from 32.00 to 58.00 wt.% does not improve considerably the electrical conductivities of these ECAs, further implying the enough high conductivity of the composite particles synthesized at C_{Ag} = 32.00 wt.%.

Table 4. Electrical conductivity of ECAs and ESCMs containing 25 vol.% of NG@Ag CSCPs synthesized in the typical experiment and flaky silver powders as conductive fillers.

Conductive fillers	Electrical conductivity of ECAs (S/m)	Electrical conductivity of ESCMs (S/m)
NG@Ag	1.73×10^4	1.99×10^4
Ag powders	6.54×10^5	1.84×10^3

Besides ECAs, as another applied materials of the conductive fillers, ESCMs have been widely applied in various fields, such as safeguard public safety, security, health and environment. ESCMs raise new requirement for these high performance conductive fillers, owing to the paint construct of this kind of coating materials. Generally, ESCMs need to be sprayed on the surface of substrate just like electrical conductive inks (ECIs) to be printed with a high resolution through nozzles[2]. For ESCMs, undesirable dispersion or sedimentation will occur if the conductive fillers have the relatively high density, resulting from the big density differences between them and polymer matrix or the low-viscosity of dispersing solvents. Most important of all, the sedimentation of the conductive fillers has a great adverse influence on the various performances of ESCMs, which significantly decreases their

electrical conductivity, shielding effectiveness (*SE*) and mechanical properties as well. As is shown in Figure S9a and b (ESI†), two pieces of ESCMs (180×180 mm) containing NG@Ag CSCPs synthesized in the typical experiment and flaky silver powders are prepared, respectively. In Table 4, the electrical conductivity of ECAs containing flaky silver powders reach up to 6.54×10^5 S/m, implying that no obvious sedimentation of flaky silver powders occurs, originating from the small density difference between silver powders and polymer matrix or the relatively high viscosity of the polymer matrix. Electrical conductivity of ESCMs containing the as-synthesized core-shell composite particles is almost same as that of their ECAs, whereas electrical conductivity of ESCMs containing flaky silver powders is two orders of magnitude smaller than that of their own ECAs. Silver powders have the high density (10.49 g/cm^3), resulting in their sedimentation in low-viscosity ESCMs before the solidification.

The SE_{total} is the summation of shielding effectiveness due to absorption (SE_A), reflection (SE_R) and multiple internal reflections (SE_M), i.e., $SE_{\text{total}} = SE_A + SE_R + SE_M$. SE_M can be negligible when $SE_{\text{total}} \leq$ -10 dB. According to Schelkunoff's electromagnetic shielding theory, equation (8) and (9) are developed to quantify the contribution of absorption and reflection to the SE_{total},[59]

$$SE_A = -0.131t\sqrt{f\mu_r\sigma_r} \quad (8)$$

$$SE_R = -168.1 + 10\lg(\frac{f\mu_r}{\sigma_r}) \quad (9)$$

where t, σ_r, μ_r and f are thickness (mm), relative conductivity, relative permeability of shielding materials and the frequency of electromagnetic wave (Hz), respectively.

Since ESCMs in this paper are non-magnetic materials, its μ_r is considered to be 1. The above equations suggest that electrical conductivity is a considerably governing parameter in terms of SE_A and SE_R.[59] Both SE_A and SE_R increase with the increasing of σ_r if other parameters of the shielding coating material are kept constantly. *SE* of ESCMs based on NG@Ag CSCPs is stronger than that of silver powder ESCMs with the frequency of electromagnetic wave ranging from 0.03 to 1.50 GHz in Figure 8. It is responsible for the sedimentation of silver powders during the solidification of ESCMs, and increasing extremely the resistivity of their ESCMs. This result shows good agreement with electric property analysis of ESCMs of silver powders.

Table 5. Mechanical properties of ECAs containing 25 vol.% of NG@Ag CSCPs synthesized in the typical experiment.

Fillers	Flexibility (mm) (GB/T 1731-1993)	Impact resistance (Kg·cm) (GB/T1732-1993)	Cross-hatch Adhesion (level) (GB/T 9286-1998)
NG@Ag	1	Direct 50 Indirect 40	0

In Table 5, its flexibility is 1 mm (Figure S10, ESI†). After the ECAs were impacted, no cracking or peeling occurred. The results of samples' direct and indirect impact resistance are 50 and 40 Kg·cm (Figure S11, ESI†), respectively. Its adhesive force is the zero level (Figure S12, ESI†). 1 mm of flexibility and zero level of adhesion are the best results in these national standards, respectively. On the

other hand, all of results show that this kind of ECAs have excellent mechanical properties, originating from the preferable dispersity of as-synthesized composite particles in polymer matrixes.

According to GJB 150.3-1986 (Enviromental Test Method for Military Equipments - High Temperature Test), the electrical conductivity of ECAs containing as-synthesized composite particles were measured at 70 ^{o}C with a time evolution (Figure S13, ESI†). After 96 h, no cracking, bubbling or peeling was observed in all ECAs samples, and their electrical conductivity still remained 1.86×10^{4} S/m or so, which is responsible for the excellent chemical stability of as-synthesized composite particles.

CONCLUSIONS

In conclusion, we have developed a facile strategy for grafting dense thiol groups on surface of NGPs as the intermediate medium to deposit thin and compact Ag shells by electroless silver plating. In our protocol, the addition of water and ammonia in the modification promotes free MPTMS molecules not only to dehydrate with hydroxyl groups on NGPs, but also to self-polymerize with the MPTMS molecules anchored on the surface of NGPs. Simply changing $V_{H_2O}:V_{MPTMS}$ regulates N_{SH} to reach up to 51.62 nm^{-2}, which substantially enhances N_{Ag}. It favors to form thin and compact silver shells on the surface of NGPs. The as-synthesized NG@Ag CSCPs show an electrical conductivity as big as 1.71×10^{6} S/m at the Ag content of 32 wt.% (corresponding to d_{Ag} of ~ 50 nm). Our results provide a novel

surface-functionalization method to graft dense thiol groups on the surface of NGPs, which offers an effective strategy to fabricate conductive fillers with big conductivity, low density, high thermal stability and low cost. Moreover, the composite materials based on the as-synthesized composite particles possess such advantages as strong shielding effectiveness, excellent anti-sedimentation, superior mechanical properties, long-term conducting stability and low filling volume percentage, promising the important applications of the as-synthesized NG@Ag CSCPs in conductive and electromagnetic shielding composite materials.

ASSOCIATED CONTENT

Electronic supplementary information (ESI) available: Size distribution of NGPs; titration curves of oxalic acid solution (black line), oxalic acid containing NGPs mixture (red line). The pH value at point A is equal to that at the initial point of red line. Point C is the start of the overlapping point of these two titration curves; Density of hydroxyl or silane on the different inner-core particles modified by trimethoxysilane; nitrogen adsorption-desorption isotherms of NGPs, MNGPs-3, MNGPs-6 and MNGPs-8; SEM images of (a) NGPs and (b) MNGPs synthesized at C_{MPTMS} = 52.0 mmol/L; (a) Low magnification and (b) high magnification SEM images of MNGPs synthesized at C_{H_2O} = 37.07 mol/L; influence of MNGPs with various N_{SH} of (a) 0.80, (b) 1.06, (c) 10.11, (d) 17.56 and (e) 28.74 nm^{-2} on the morphology of the as-synthesized NG@Ag CSCPs, other conditions as the typical experiment except for functionalization of NGPs. The insets show the corresponding

high magnification images of these composite particles; influence of N_{SH} of MNGPs on N_{Ag} of NG@Ag CSCPs; cross-section morphology of NG@Ag CSCPs synthesized at respective V_A of (a) 34.0, (b) 50.0 and (c) 64.0 mL, other conditions as the typical experiment except for V_A. Scale bars are all 100 nm; photographs of ESCMs containing 25 vol.% of (a, c) NG@Ag CSCPs and (b, d) flaky silver powders, respectively. (e) Photograph to show the coaxial fixture of shielding effectiveness test. As is shown in Figure S9, two pieces of ESCMs (180×180 mm) containing (a) NG@Ag CSCPs synthesized in the typical experiment and (b) flaky silver powders are prepared, respectively. Two pieces of ESCMs (annular wafer with outer radius of 55.00 mm, inner radius of 6.25 mm and thickness about 150 μm) containing (c) NG@Ag CSCPs and (d) flaky silver powders were patterned by an engraving machine, respectively. The scale bars in (a) and (b) are 100 mm; the scale bars in (c) and (d) are 25 mm; photographs of ECAs determination for flexibility as GB/T 1731-1993 standards, the volume fraction of as-synthesized composite particles as Figure S9**.** ECAs were coated on tinplate panels of 15 cm × 2.5 cm, its thickness is 200 μm; photograph of ECAs determination for impact resistance as GB/T 1732-1993 standards, the volume fraction of as-synthesized composite particles as Figure S9. The direct and indirect impact resistance are indicated by the region A and region B, respectively. ECAs were coated on tinplate panels of 15 cm × 5 cm, its thickness is 200 μm. The scale bar is 20 mm; photograph of ECAs determination for cross-hatch adhesion as GB/T 9286-1998 standards, the volume fraction of as-synthesized composite particles as Figure S9. ECAs were coated on FR-4 panels of 18 cm × 7 cm,

its thickness is 200 μm. The scale bar is 5 mm; effect of aging time on the electrical conductivity of ECAs, the volume fraction of as-synthesized composite particles as Figure S9.

Notes

The authors declare no competing financial interest.

ACKNOWLEDGMENT

This work was supported by the National Natural Science Foundation of China (21474078, 51521001 and 51577138), the Top Talents Lead Cultivation Project of Hubei Province, the Natural Science Foundation of Hubei Province (2014CFB163 and 2015CFA003), the Yellow Crane Talents Plan of Wuhan Municipal Government, the Fundamental Research Funds for the Central Universities (WUT: 2014-IV-131) and the Self-Determined and Innovative Research Funds of Wuhan University of Technology (2014-Ia-032).

REFERENCES

1. Z. Huang, B. Chi, J. Guan and Y. Liu, *RSC Adv.*, 2014, **4**, 18645.
2. C. Yang, C. P. Wong and M. M. F. Yuen, *J. Mater. Chem. C*, 2013, **1**, 4052.
3. M. Lan, D. Zhang, J. Cai, Y. Hu and L. Yuan, *Appl. Surf. Sci.*, 2014, **307**, 287.
4. K.-H. Chen, Y.-C. Pu, K.-D. Chang, Y.-F. Liang, C.-M. Liu, J.-W. Yeh, H.-C. Shih and Y.-J. Hsu, *J. Phys. Chem. C*, 2012, **116**, 19039.

5. Y. Zhang, X. Yuan, Y. Wang and Y. Chen, *J. Mater. Chem.*, 2012, **22**, 7245.

6. S. K. Li, Y. X. Yan, J. L. Wang and S. H. Yu, *Nanoscale*, 2013, **5**, 12616.

7. J. K. Yang, H. Kang, H. Lee, A. Jo, S. Jeong, S. J. Jeon, H. I. Kim, H. Y. Lee, D. H. Jeong, J. H. Kim and Y. S. Lee, *ACS Appl. Mater. Interfaces*, 2014, **6**, 12541.

8. Y. Wang, Q. Zhang, H. Shao and J. Guan, *Chin. J. Struct. Chem.*, 2010, **29**, 555.

9. L. He and S. C. Tjong, *RSC Adv.*, 2015, **5**, 15070.

10. Y. Hu, T. Zhao, P. Zhu, X. Liang, R. Sun and C.-P. Wong, *RSC Adv.*, 2015, **5**, 58.

11. H.-Y. Chen, H.-P. Shen, H.-C. Wu, M.-S. Wang, C.-F. Lee, W.-Y. Chiu and W.-C. Chen, *J. Mater. Chem. C*, 2015, **3**, 3318.

12. S. Kalele, S. Gosavi, J. Urban and S. Kulkarni, *Curr. Sci.*, 2006, **91**, 1038.

13. S. Tang, Y. Tang, S. Zhu, H. Lu and X. Meng, *J. Solid State Chem.*, 2007, **180**, 2871.

14. V. G. Pol, D. N. Srivastava, O. Palchik, V. Palchik, M. A. Slifkin, A. M. Weiss and A. Gedanken, *Langmuir*, 2002, **18**, 3352.

15. K. Wang, X. Zhang, C. Niu and Y. Wang, *ACS Appl. Mater. Interfaces*, 2014, **6**, 1272.

16. M. McKiernan, J. Zeng, S. Ferdous, S. Verhaverbeke, K. S. Leschkies, R. Gouk, C. Lazik, M. Jin, A. L. Briseno and Y. Xia, *Small*, 2010, **6**, 1927.

17. T. Cassagneau and F. Caruso, *Adv. Mater.*, 2002, **14**, 732.

18. A. G. Dong, Y. J. Wang, Y. Tang, N. Ren, W. L. Yang and Z. Gao, *Chem. Commun.*, 2002, DOI: 10.1039/b110164c, 350.

19. L. Tongxiang, G. Wenli, Y. Yinghui and T. Chunhe, *Int. J. Adhes. Adhes.*, 2008, **28**, 55.

20. Y. Ma and Q. Zhang, *Appl. Surf. Sci.*, 2012, **258**, 7774.

21. J. Zhang, J. Liu, S. Wang, P. Zhan, Z. Wang and N. Ming, *Adv. Funct. Mater.*, 2004, **14**, 1089.

22. W. Wang, R. Li, M. Tian, L. Liu, H. Zou, X. Zhao and L. Zhang, *ACS Appl. Mater. Interfaces*, 2013, **5**, 2062.

23. Y. Fu, L. Liu, L. Zhang and W. Wang, *ACS Appl. Mater. Interfaces*, 2014, **6**, 5105.

24. W. G. Choe, D. Y. Kim and O. O. Park, *CrystEngComm*, 2014, **16**, 5142.

25. G. Chen, W. Weng, D. Wu, C. Wu, J. Lu, P. Wang and X. Chen, *Carbon*, 2004, **42**, 753.

26. C. Li, X. Gong, L. Tang, K. Zhang, J. Luo, L. Ling, J. Pu, T. Li, M. Li and Y. Yao, *J. Mater. Chem. C*, 2015, **3**, 6178.

27. Y. Wei, S. Chen, Y. Lin, Z. Yang and L. Liu, *J. Mater. Chem. C*, 2015, **3**, 9594.

28. S. Zhao, J. Chen and Y. Wang, *Acta Metall.*, 2012, **48**, 977.

29. F. He, S. Lau, H. L. Chan and J. Fan, *Adv. Mater.*, 2009, **21**, 710.

30. Y. P. Wu, C. Jiang, C. Wan and R. Holze, *J. Power Sources*, 2002, **111**, 329.

31. K. A. Striebel, A. Sierra, J. Shim, C. W. Wang and A. M. Sastry, *J. Power Sources*, 2004, **134**, 241.

32. R. Xu, J. He, Y. Song, W. Li, A. Zaslavsky and D. C. Paine, *Appl. Phys. Lett.*, 2014, **105**, 093504.

33. W. Sun, G. Chen and L. Zheng, *Scripta Mater.*, 2008, **59**, 1031.

34. Y. Zhang, S. Qi, X. Wu and G. Duan, *Synth. Met.*, 2011, **161**, 516.

35. L. Zhao, H. Ma and J. Guan, *Chem. J. Chinese Universities*, 2009, **30**, 1454.

36. M. L. Toebes, J. M. P. van Heeswijk, J. H. Bitter, A. Jos van Dillen and K. P. de Jong, *Carbon*, 2004, **42**, 307.

37. M. K. van der Lee, J. van Dillen, J. H. Bitter and K. P. de Jong, *J. Am. Chem. Soc.*, 2005, **127**, 13573.

38. D. Zhao, C. Chen, Y. Wang, H. Ji, W. Ma, L. Zang and J. Zhao, *J. Phys. Chem. C*, 2008, **112**, 5993.

39. F. Bauer, H. Ernst, D. Hirsch, S. Naumov, M. Pelzing, V. Sauerland and R. Mehnert, *Macromol. Chem. Phys.*, 2004, **205**, 1587.

40. Y. Zhou, R. Huang, F. Ding, A. D. Brittain, J. Liu, M. Zhang, M. Xiao, Y. Meng and L. Sun, *ACS Appl. Mater. Interfaces*, 2014, **6**, 7417.

41. L. SelegArd, V. Khranovskyy, F. Soderlind, C. Vahlberg, M. Ahren, P. O. Kall, R. Yakimova and K. Uvdal, *ACS Appl. Mater. Interfaces*, 2010, **2**, 2128.

42. H. Li, R. Wang, H. Hu and W. Liu, *Appl. Surf. Sci.*, 2008, **255**, 1894.

43. D. H. K. Jackson, D. Wang, J. M. R. Gallo, A. J. Crisci, S. L. Scott, J. A. Dumesic and T. F. Kuech, *Chem. Mater.*, 2013, **25**, 3844.

44. J. I. Paredes, S. Villar-Rodil, A. Martínez-Alonso and J. M. D. Tascón, *Langmuir*, 2008, **24**, 10560.

45. F. A. Silva and F. L. Pissetti, *J Colloid Interface Sci*, 2014, **416**, 95.

46. N. D. Meeks, E. Davis, M. Jain, G. Skandan and D. Bhattacharyya, *Environ. Prog. Sustainable Energy*, 2013, **32**, 705.

47. C. Bressy, V. G. Ngo, F. Ziarelli and A. Margaillan, *Langmuir*, 2012, **28**, 3290.

48. F. He, W. Wang, J. W. Moon, J. Howe, E. M. Pierce and L. Liang, *ACS Appl. Mater. Interfaces*, 2012, **4**, 4373.

49. T.-L. Ho, *Chem. Rev.*, 1975, **75**, 1.

50. Y. Wang, J. Wen, S. Zhao, Z. Chen, K. Ren, J. Sun and J. Guan, *Langmuir*, 2015, **31**, 13441.

51. A. Krasnoslobodtsev and S. Smirnov, *Langmuir*, 2001, **17**, 7593.

52. J. Lin, *J. Inorg. Mater.*, 1997, **12**, 363.

53. S. Ek, E. I. Iiskola, L. Niinistö, J. Vaittinen, T. T. Pakkanen, J. Keränen and A. Auroux, *Langmuir*, 2003, **19**, 10601.

54. R. Pasricha, S. Gupta and A. K. Srivastava, *Small*, 2009, **5**, 2253.

55. J. Y. Lin, B. Ding, J. Y. Yu, G. C. Wu, J. M. Yang and G. Sun, in *Int. J. Nonlinear Sci. Numer. Simul.*, 2010, vol. 11, p. 523.

56. S. Stankovich, D. A. Dikin, G. H. Dommett, K. M. Kohlhaas, E. J. Zimney, E. A. Stach, R. D. Piner, S. T. Nguyen and R. S. Ruoff, *Nature*, 2006, **442**, 282.

57. M. A. Rafiee, J. Rafiee, Z. Wang, H. Song, Z.-Z. Yu and N. Koratkar, *ACS Nano*, 2009, **3**, 3884.

58. P. Lee, J. Lee, H. Lee, J. Yeo, S. Hong, K. H. Nam, D. Lee, S. S. Lee and S. H. Ko, *Adv. Mater.*, 2012, **24**, 3326.

59. L.-C. Jia, D.-X. Yan, C.-H. Cui, X. Jiang, X. Ji and Z.-M. Li, *J. Mater. Chem. C*, 2015, **3**, 9369.

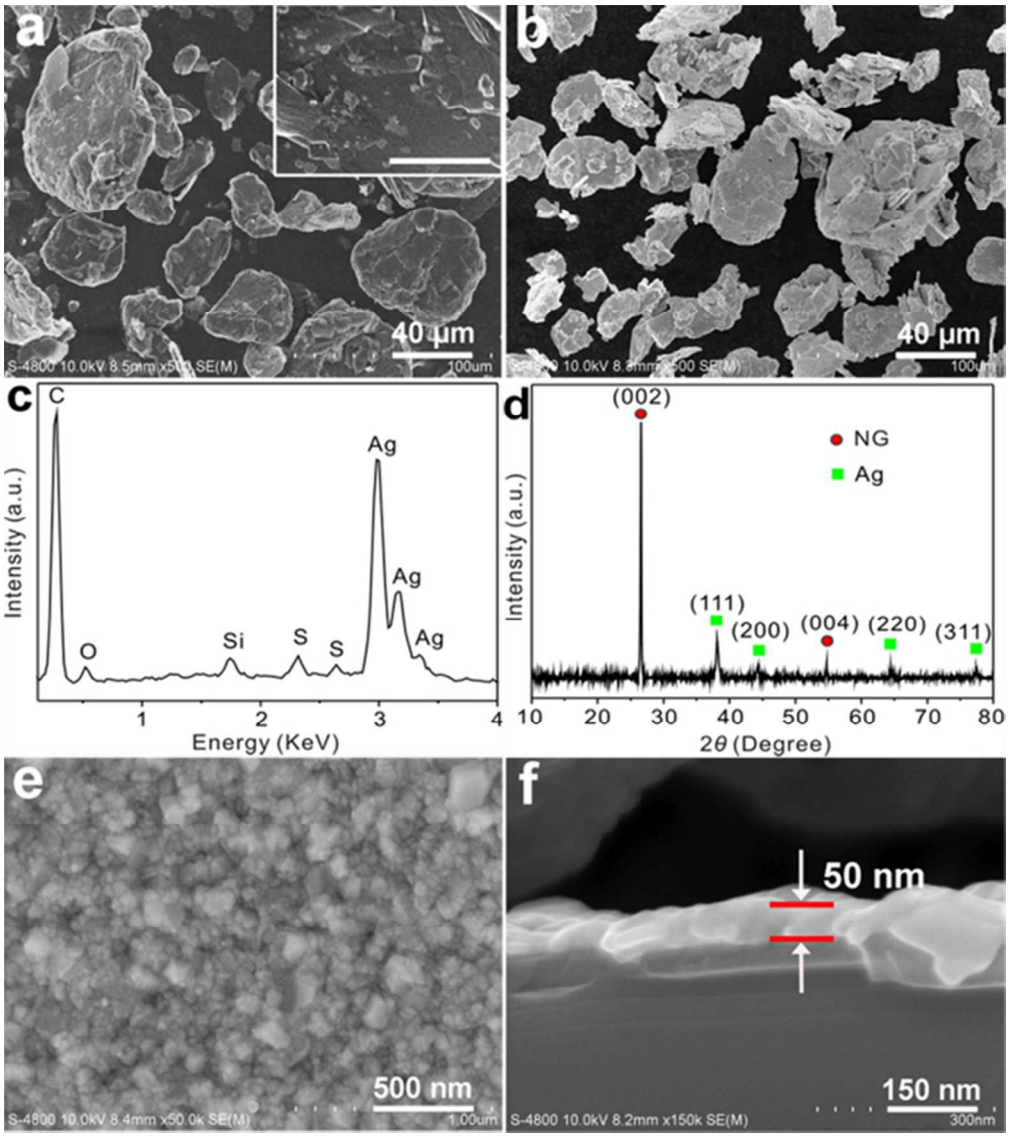

Figure 1. (a) SEM image of NGPs. (b) SEM image, (c) EDX spectrum and (d) XRD pattern of NG@Ag CSCPs synthesized in the typical experiment. (e) and (f) show the typical SEM magnified image and cross-section morphologies of NG@Ag CSCPs indicated in (b), respectively. The scale bar in the inset of (a) is 500 nm.
61x68mm (300 x 300 DPI)

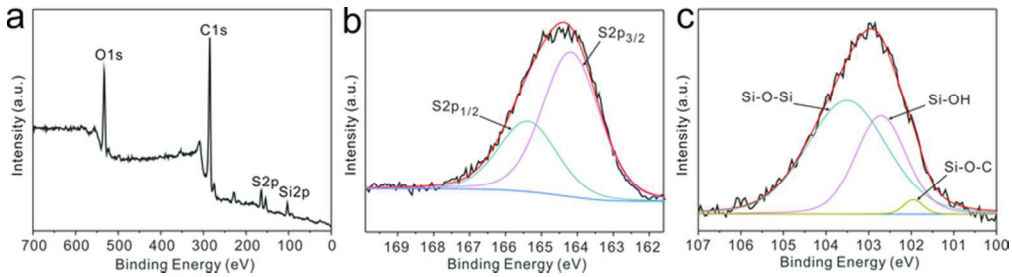

Figure 2. XPS spectra of MPTMS-functioned NGPs synthesized in the typical experiment (a) Full spectrum, (b) S2p and (c) Si2p high-resolution spectra.
72x19mm (300 x 300 DPI)

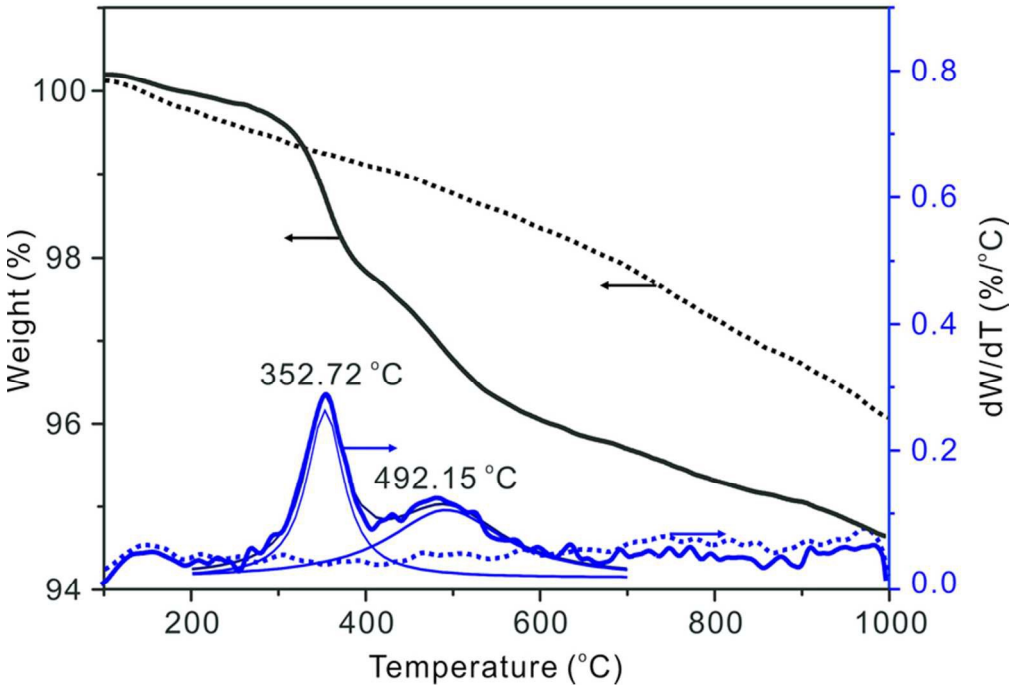

Figure 3. TG-DTG curves of NGPs (dotted line) and MNGPs (solid line). The DTG curve of MNGPs synthesized in the typical experiment from 200 to 700 °C is fitted with Gaussian function.
73x51mm (300 x 300 DPI)

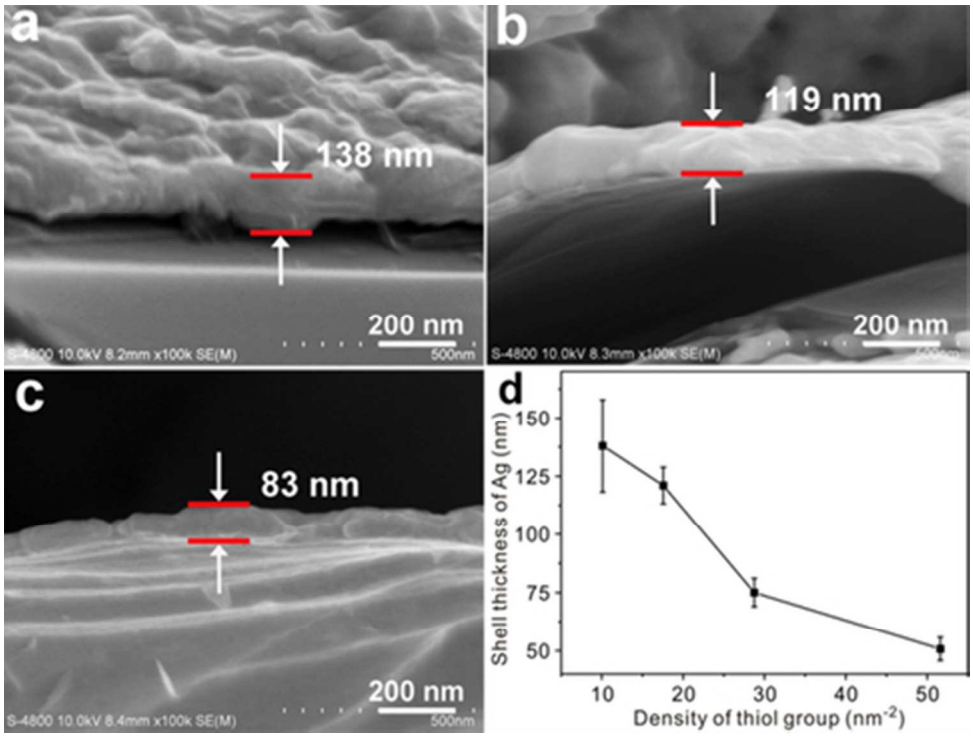

Figure 4. Cross-section SEM images of NG@Ag CSCPs synthesized at MNGPs with various N_{SH} of (a) 10.11, (b) 17.56 and (c) 28.74 nm^{-2}. (d) shows the effect of N_{SH} of MNGPs on d_{Ag} of NG@Ag CSCPs.
40x30mm (300 x 300 DPI)

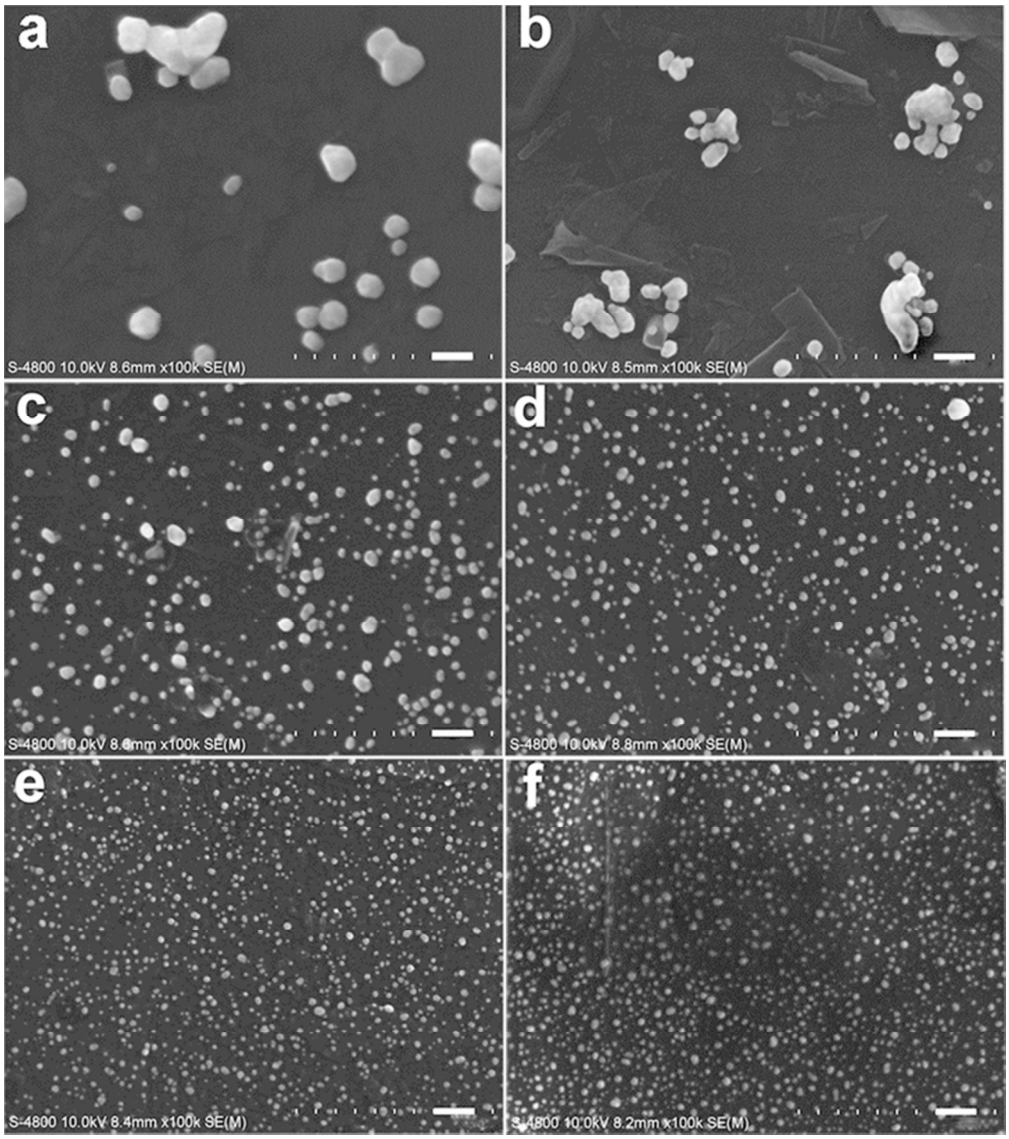

Figure 5. SEM images of NG@Ag CSCPs synthesized at MNGPs with various N_{SH} of (a) 0.80, (b) 1.06, (c) 10.11, (d) 17.56, (e) 28.74 and (f) 51.62 nm^{-2}. All NG@Ag CSCPs were synthesized at V_A = 1.00 mL. The scale bar is 100 nm.
61x69mm (300 x 300 DPI)

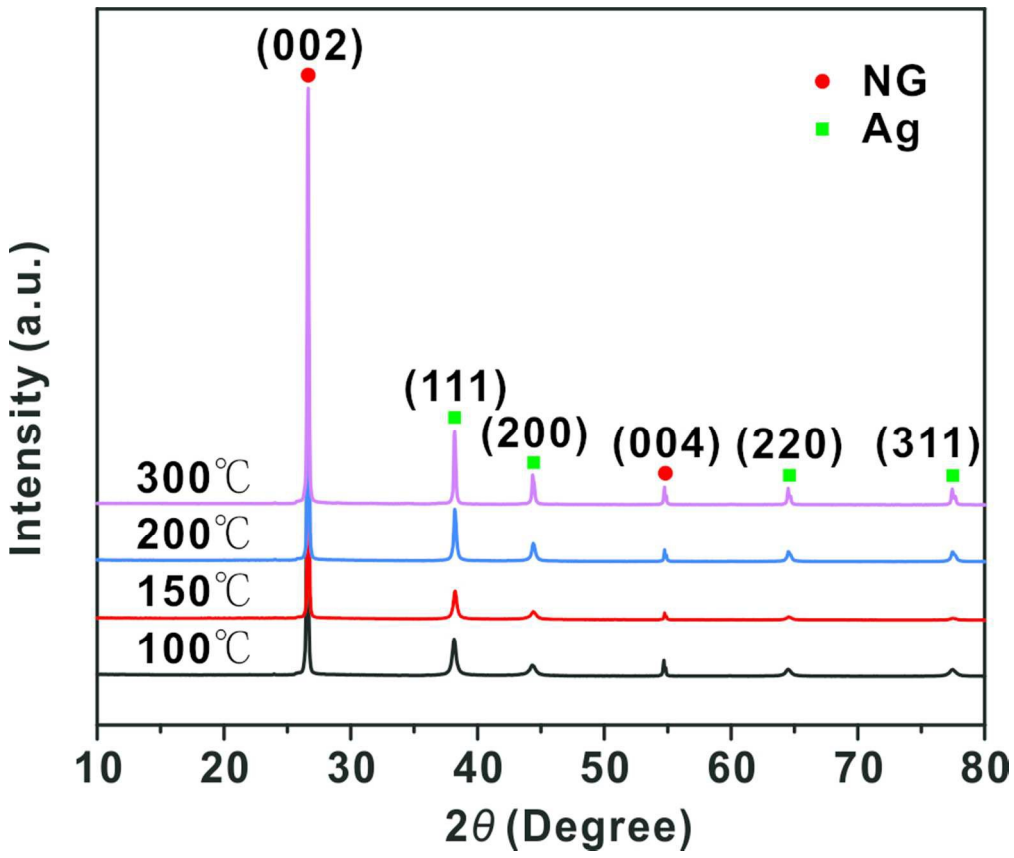

Figure 6.Influence of thermal treatment temperature on XRD patterns of NG@Ag CSCPs synthesized in the typical experiment.
83x70mm (300 x 300 DPI)

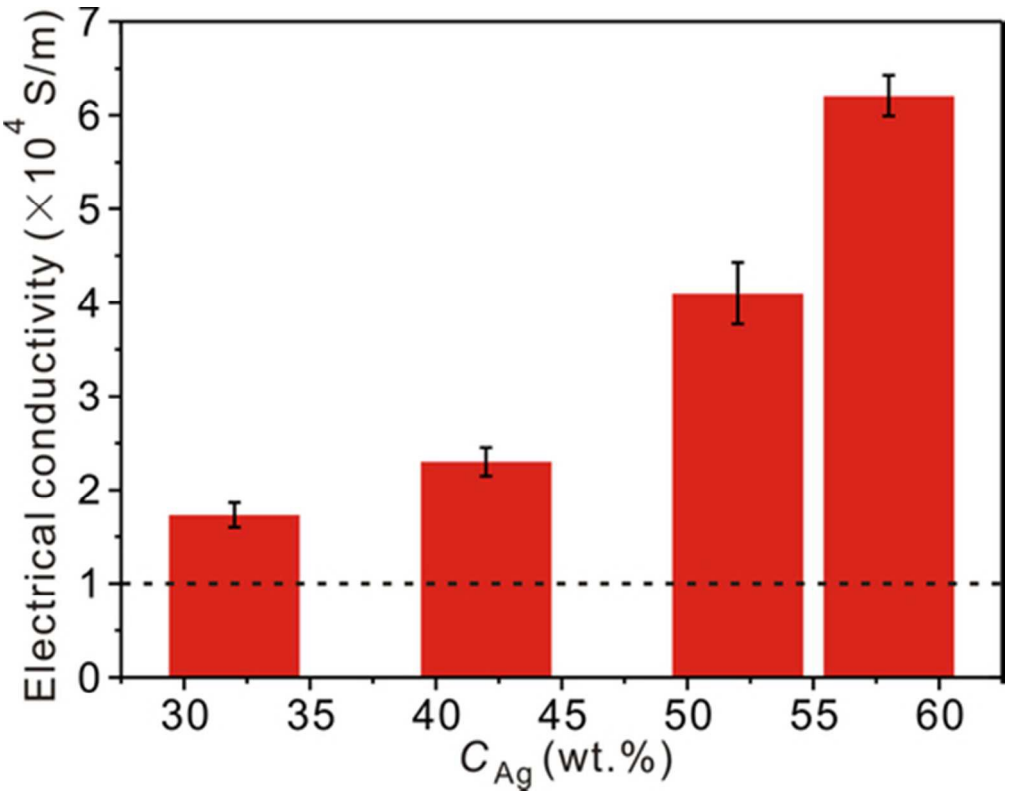

Figure 7. Electrical conductivity of ECAs containing 25.00 vol.% of NG@Ag CSCPs with various C_{Ag} of 32.00, 42.00, 52.00 and 58.00 wt.%, respectively.
42x33mm (300 x 300 DPI)

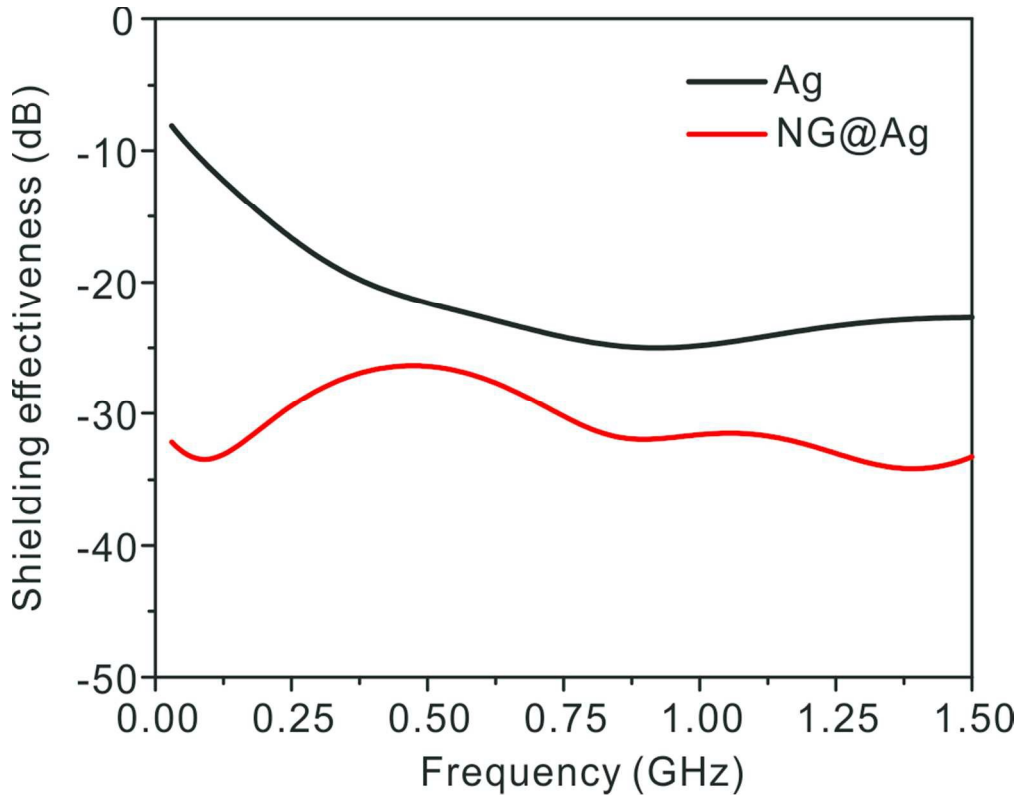

Figure 8. *SE* of ESCMs containing the as-synthesized NG@Ag CSCPs or flaky silver powders with the frequency of electromagnetic wave ranging from 0.03 to 1.50 GHz.
91x71mm (300 x 300 DPI)

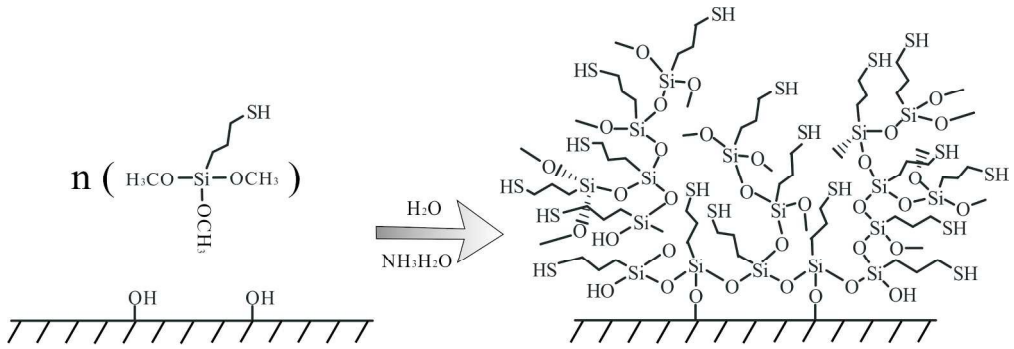

Scheme 1. Schematic illustration of the grafted thiol groups on the surface of NGPs.
208x70mm (300 x 300 DPI)

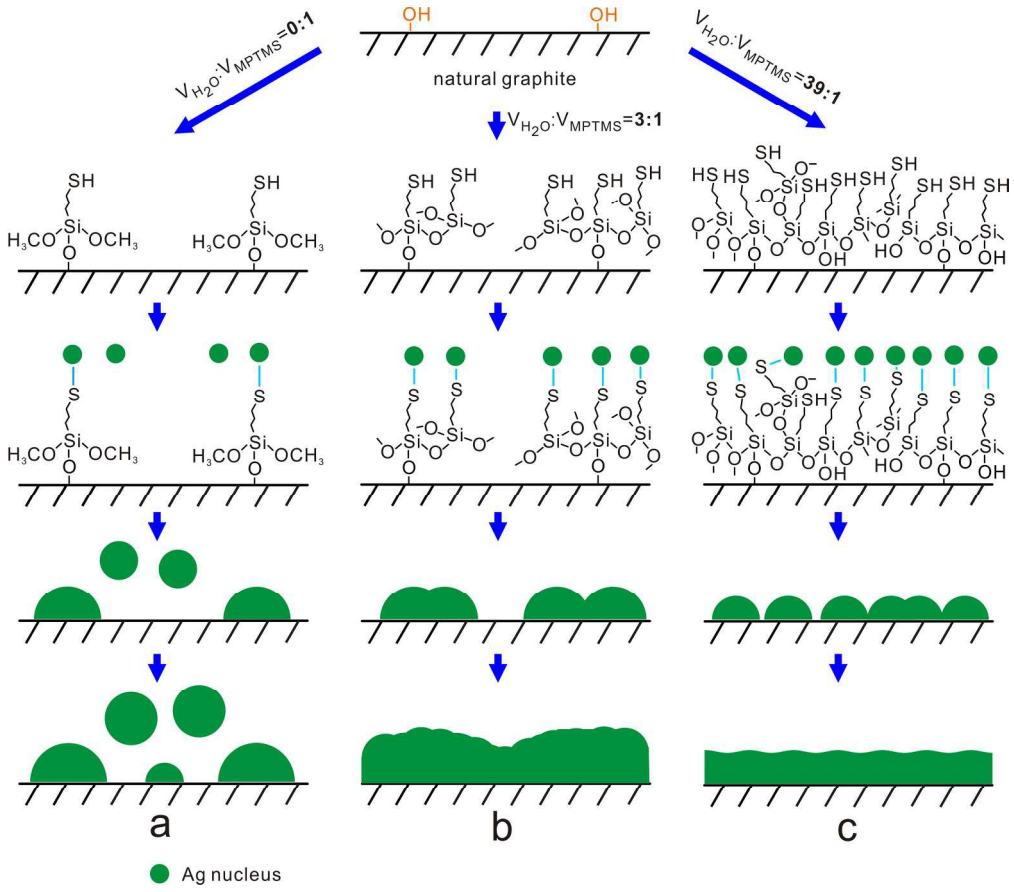

Scheme 2. Schematic representation for the formation mechanism of thin and compact Ag shells deposition on the surface of NGPs.
105x92mm (600 x 600 DPI)

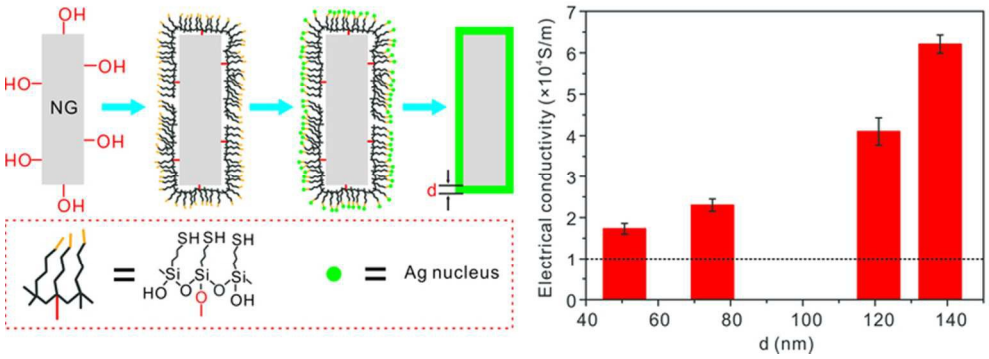

A table of contents entry: Facile synthesis of dense N_{SH} on NGPs facilitates to fabricate NG@Ag CSCPs with low silver content and high performances.
71x25mm (300 x 300 DPI)